Statistical-Topographical Mapping of Rainfall Over Mountainous Terrain Using Beta Scaling

Jan Wienhöfer[1], Lucas Alcamo[2], Jan Bondy[3], and Erwin Zehe[4]

[1]Karlsruhe Institute of Technology
[2]Technical University of Munich
[3]Deutscher Wetterdienst DWD
[4]Karlsruhe Institute of Technology KIT

May 25, 2023

Abstract

We present a robust approach for quantitative precipitation estimation (QPE) for water resources management in mountainous catchments, where rainfall sums and variability are correlated with orographic elevation, but density of rain gauges does not allow for advanced geostatistical interpolation of rainfall fields.

Key of the method is modelling rainfall at unobserved locations by their elevation-dependent expected daily mean, and a daily fluctuation which is determined by spatial interpolation of the residuals of neighbouring rain gauges, scaled according to the elevation difference. The scaling factor is defined as the ratio of covariance and variance, in analogy to the "beta" used in economics.

The approach is parameterized and illustrated for the Chirilu catchments (Chillón, Rímac, Lurín) in the Andes near Lima, Peru. The results are compared to conventional IDW (inverse-distance weighting) interpolation and a merged national rainfall product. The method results in QPE that are better matching with observed discharges. The combination of inverse-distance weighting with β-scaling thus provides a robust and flexible means to estimate rainfall input to mesoscale mountainous catchments.

Hosted file

962719_0_art_file_10959009_rb5dr2.docx available at https://authorea.com/users/616093/articles/642223-statistical-topographical-mapping-of-rainfall-over-mountainous-terrain-using-beta-scaling

Statistical-Topographical Mapping of Rainfall Over Mountainous Terrain Using Beta Scaling

Jan Wienhöfer[1], Lucas Alcamo[1]*, Jan Bondy[1‡], and Erwin Zehe[3]

[1]Karlsruhe Institute of Technology (KIT), Institute for Water and River Basin Management (IWG), Chair of Hydrology, Kaiserstraße 12, 76131 Karlsruhe, Germany.

Corresponding author: Jan Wienhöfer (jan.wienhoefer@kit.edu)

* current address: Chair of Hydrology and River Basin Management, Technical University of Munich, Arcisstrasse 21, 80333 München, Germany

‡ current address: Deutscher Wetterdienst (DWD), Frankfurter Str. 135, 63067 Offenbach am Main, Germany.

Key Points:

- A simple, yet effective way of mapping rainfall over mountain catchments is developed and tested for catchments in the Andes near Lima, Peru
- A scaling factor depending on the difference in elevation to observation stations is defined in analogy to the “beta” used in economics
- Beta scaling extrapolates rainfall trends to higher, unobserved elevations, and provides more consistent estimates of catchment rainfall

Abstract

We present a robust approach for quantitative precipitation estimation (QPE) for water resources management in mountainous catchments, where rainfall sums and variability are correlated with orographic elevation, but density of rain gauges does not allow for advanced geostatistical interpolation of rainfall fields.

Key of the method is modelling rainfall at unobserved locations by their elevation-dependent expected daily mean, and a daily fluctuation which is determined by spatial interpolation of the residuals of neighbouring rain gauges, scaled according to the elevation difference. The scaling factor is defined as the ratio of covariance and variance, in analogy to the "beta" used in economics.

The approach is parameterized and illustrated for the Chirilu catchments (Chillón, Rímac, Lurín) in the Andes near Lima, Peru. The results are compared to conventional IDW (inverse-distance weighting) interpolation and a merged national rainfall product. The method results in QPE that are better matching with observed discharges. The combination of inverse-distance weighting with ß-scaling thus provides a robust and flexible means to estimate rainfall input to mesoscale mountainous catchments.

1 Introduction

Mapping the precipitation patterns for terrain with complex topography can be a challenging task that is crucial for a broad range of applications in water resources management, including hydrological and water quality modeling, as well as for crop production modelling and ecological studies.

Estimates of spatially distributed precipitation are typically based on rain gauge measurements, which are interpolated over the region of interest (Michaelides et al., 2009). Remote sensing methods are increasingly employed to estimate spatially distributed rainfall, but are known to be less reliable for quantitative estimates, especially in the case of satellite-based products (AghaKouchak et al., 2011). The quality of satellite-derived rainfall estimates varies across different climate and topographic settings as well as across space-time scales, and tends to be more reliable in humid areas and flat terrain (Anagnostou, 2004; Hu et al., 2019). Ground-based remote sensing methods such as radar observations can achieve higher accuracies (Neuper & Ehret, 2019), but are also limited in their applicability in mountainous regions (Germann et al., 2006; Young et al., 1999). The limited detection range and considerable costs of radar stations are further reasons why radar-based rainfall measurements may not be available in a particular region. Costs for installation and regular maintenance similarly affect the availability and data quality of classical rain gauge measurements, causing the data coverage to vary greatly across the globe, especially in mountainous areas. The installation of new rain gauges is an option to collect (additional) site-specific rainfall data (e.g., Buytaert et al., 2006; Michelon et al., 2021; Wienhöfer et al., 2011), but this involves considerable efforts in remote mountainous areas, and is usually limited by available funding.

The total rainfall amount across a catchment is determined from these measurements in a procedure referred to as quantitative precipitation estimation (QPE). In many cases, the QPE is based on an interpolation of rain gauge measurements, possibly considering other auxiliary data. The most widely used methods for spatial interpolation include deterministic approaches like Thiessen polygons or inverse-distance weighting (IDW), and probabilistic approaches like kriging and related geostatistical methods (see review articles by Li & Heap, 2014; Ly et al., 2013; Sluiter, 2009).

The basic, univariate versions of these methods use the value of interest and their geographical distances to interpolate to an unobserved location. Thiessen polygons simply take the value of the nearest station. The IDW method uses a weighted average of nearby stations, where the weights decrease with the distance of the stations. Kriging methods also use a weighted combination of observed values. The kriging weights are calculated using the theoretical variogram function, which indicates the decrease in statistical dependence as the distance between points increases. This function is equivalent to spatial covariance when second-order stationarity is assumed (for an in-depth treatment of geostatistical approaches see, e.g., Webster & Oliver, 2007). Kriging is computationally more intensive, but offers the advantages of minimized estimation variance and prediction error estimates, if the underlying statistical assumptions are met.

Generally, the choice of the interpolation method depends on the spatial scale, the density of the observation network, the topography of the area, and the nature of the variable to be interpolated (Herrera et al., 2019; Ly et al., 2013). Although many studies identified kriging as the favorable method for rainfall interpolation in different settings (e.g., Belo-Pereira et al., 2011; Campling et al., 2001; Hofstra et al., 2008), it is not necessarily the best method for all situations. A similar performance of kriging and IDW was reported by other researchers, for example when interpolating daily rainfall in two catchments of about 3000 km² in Belgium (Ly et al., 2011). Dirks et al. (1998) found that kriging did not outperform the inverse-distance, Thiessen, and simple average methods in their study of a high-density network of rain gauges on a Pacific island (13 gauges per 35 km²), because meaningful variograms for kriging could neither be found at daily nor at longer intervals. Rainfall interpolated with IDW was found to deliver more consistent results when used in hydrological models in a data-scarce region in West Africa (13 gauges per 100,000 km²), as compared to rainfall estimates obtained with kriging or Thiessen polygons (Ruelland et al., 2008).

Using multivariate techniques that consider the spatial correlations between rainfall and other relevant proxy variables can help to improve estimations of actual rainfall patterns. When both radar data proxies and rainfall gauges are available, the two data sources can be merged for the spatial interpolation, such that the spatial variability from radar images and quantitative information from gauge measurements are combined (e.g., Ehret et al., 2008; Heistermann & Kneis, 2011; see also the review article by Hu et al., 2019). Proxy information from satellite-based rainfall estimates and atmospheric reanalysis can be incorporated in a similar manner, but the resulting global datasets offer a coarser spatial resolution and show large random errors and strong biases (Sun et al., 2018), which still limits their applicability for QPE at the catchment scale. For example, Scheel et al. (2011) reported only a modest correlation ($r < 0.5$) of satellite-derived rainfall and ground observations for two study sites in the Central Andes.

Since spatial variation of rainfall can be strongly related to the local and regional orography (Roe, 2005), QPE at the local or regional scale can benefit from information on physiographic characteristics, for example from digital elevation models (DEMs). This topographic information can be included with different methods, ranging from pure regression techniques, over regression with spatial interpolation of the residuals, to more complex, multivariate geostatistical methods like external drift kriging, which accounts for a spatial drift of the mean values, or cokriging, which uses the variograms and the cross-variogram of the primary and secondary variables. For example, linear regression with orographic elevation is used by PRISM (Precipitation elevation Regressions on Independent Slopes Model) to estimate monthly and annual precipitation sums on individual "topographic facets" with similar slope orientation (Daly et al., 1994). PRISM includes smoothing of the DEM to determine the facets and the orographic elevation of the stations used in regression. The authors found that PRISM yielded lower cross-validation errors compared to geostatistical methods (kriging, detrended kriging, and cokriging) when applied to the Willamette River basin (Oregon, USA; basin size 29,730 km²). Goovaerts (2000) compared different methods for incorporating elevation into the spatial interpolation of monthly and annual rainfall in Southern Portugal. Approaches that are combining linear regression estimates of mean rainfall from elevation with interpolation of the residuals (simple kriging with varying local means, kriging with external drift) were found to work better than the more complex multivariate cokriging, or the more simple pure linear regression. Buytaert et al. (2006) investigated rainfall patterns in three small catchments in the South Ecuadorian Andes with multivariate regression. They found that interpolation of the residuals with kriging performed slightly better than using Thiessen polygons, but, more importantly, they also showed that including correlations of rainfall with topography outweighed the effects of different interpolation methods.

A general conclusion from the reviewed literature is that a chosen QPE method should be specific to a particular catchment, and needs to reflect both the local conditions determining the rainfall patterns and the temporal and spatial coverage of rainfall observations. The available data need to be carefully analyzed for spatial covariance and correlation with topography, and the method of rainfall interpolation should then be chosen such that relationships present in the dataset are exploited in the best possible way.

Here, we investigate catchment rainfall input in the Chirilu area, which encompasses the Chillón, Rímac, and Lurín watersheds near Lima, Peru. The objectives of the study are i) to analyze spatial and statistical relationships among daily rainfall data; ii) to develop a reliable interpolation method for rainfall using the identified relationships; and iii) to evaluate the performance of the developed method through cross-validation and comparisons with the conventional IDW interpolation and the Peruvian rainfall product PISCO as benchmarks.

The paper is organized as follows. Relevant information about the study area, the data, and implementation are summarized in section 2. The statistical relationships of rainfall and topography and the rainfall interpolation model are detailed in sections 3 and 4, respectively. The results of the rainfall interpolation and evaluation are presented and discussed in section 5. Section 6 summarizes the study and offers conclusions.

2 Materials and Methods

2.1 Study area

The study area is located on the western slopes of the Peruvian Andes in South America between 11.3° to 12.3°S and 76.0° to 77.2°W. It encompasses the neighboring catchments of the

Chillón, Rímac and Lurín Rivers (Chirilu). The three rivers drain an area of approximately 7 300 km^2, and discharge into the Pacific Ocean. The catchments are of particular interest as the Peruvian capital Lima strongly relies on water supply from this region (Lavado Casimiro et al., 2012). Most of the water delivers the Rímac River, which is heavily supplemented with water from the much larger Mantaro catchment through transandine tunnels.

The steep topographic gradient in the region, from around 5500 m a.s.l. at the Andes crest down to sea level over a distance of 100 km, conditions distinct climate zones throughout the basins. The climate ranges from extremely arid and arid in the lower coastal parts (0 to 1500 m a.s.l.) to semi-arid and semi-humid in the middle and upper parts (1500 to 5000 m a.s.l.). A few snow-covered and glacial areas are located at the highest elevations. Mean annual precipitation at the coast is less than 20 mm as opposed to around 800 mm in the highest parts of the basin (Observatorio del Agua Chillón Rímac Lurín, 2019). The aridity of the coastal region results from a quasi-permanent inversion of the lower atmosphere due to large-scale subsidence of air masses. The inversion layer effectively inhibits convection, and thus cloud and rainfall formation in the lower region, while precipitation in the highlands of the western slopes are mainly induced by advection of air masses from the east across the Amazon basin (Garreaud, 2009; Trachte et al., 2018). Temporal precipitation patterns show a distinct seasonality, with the main rainy season during the austral summer months December through February, as well as a dry season during the austral winter June through August.

2.2 Data and preprocessing

2.2.1 Rain gauges

For this study, daily precipitation data from a total of 67 rain gauges at various altitudes were available (Figure 1). The rainfall dataset covers nearly 57 years from August 1963 until January 2020, and contains station located between 24 m and 4764 m a.s.l. Rainfall data from 62 stations were kindly provided by the Observatorio del Agua Chillón Rímac Lurín. To collect additional data in unobserved parts, we installed five new stations (herein referred to as “IWG stations”) in the headwater catchments of the Lurín: two rain gauges in November 2017, one of which was operational only until May 2018, and the other three were installed in November/December 2018.

However, the records of the 67 stations vary in length and include data gaps. The median number of stations available per day is 24, with a minimum of 2 and a maximum of 42 stations. The rain gauge data was aggregated to monthly and annual totals including only complete series. Only 16 of the stations have data for 360 or more months; 38 stations have data for 60 or more months. The aggregated data of 16 stations with records equivalent to 30 years of observation were used to assess the rainfall climatology, especially the relationships with topography, and spatial patterns presented in section 3. These 16 stations are located between 527 m and 4169 m a.s.l.

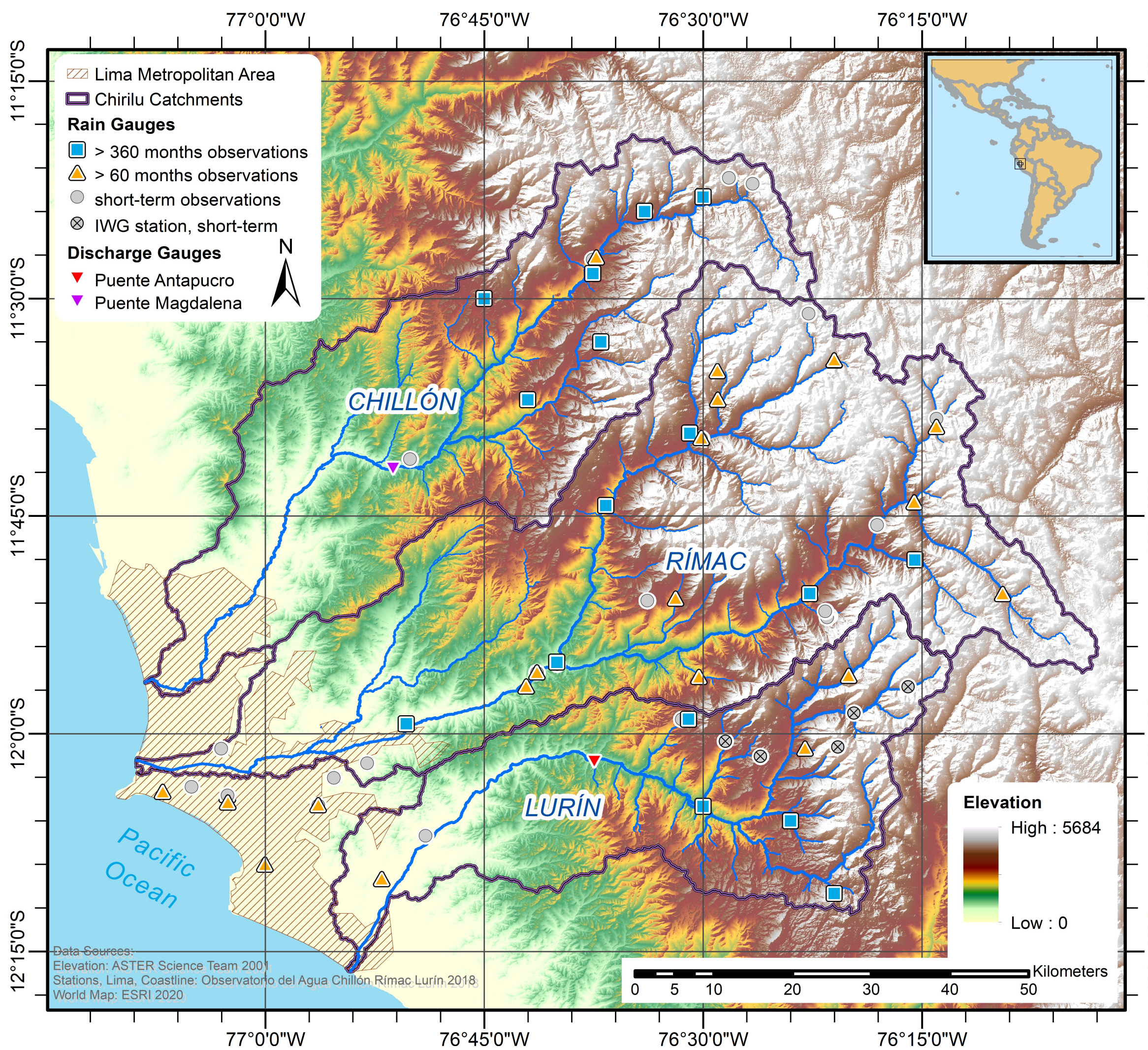

Figure 1: Overview map of the Lima area and the Chillón, Rímac and Lurín (Chirilu) catchments. 67 rain gauges have been used in the analysis: 16 stations have more than 360 months of data, and additional 22 rain gauges have more than 60 months of data. The other are short-term stations, of which five were set up at higher elevations in the Lurín headwaters (IWG stations). The locations of discharge gauges Puente Magdalena and Puente Antapucro are also shown.

2.2.2 PISCO precipitation product

The PISCO dataset (Peruvian Interpolated data of SENAMHI's Climatological and Hydrological Observations) is a national gridded data product provided by the Peruvian Meteorological and Hydrological National Service (SENAMHI) that covers the entire country of Peru at a spatial resolution of 0.1°. Precipitation data is available at daily and monthly resolution. We have used version "PISCO Prec v2p1 stable daily" (1981 to 2016) and "PISCO Prec v2p1 unstable monthly" (1981 to 2021), hereinafter referred to as daily and monthly PISCO, respectively. PISCO determines precipitation based on data from three different sources: the national quality-controlled and infilled rain gauge data set, climatologies based on satellite data (TRMM), and the Climate Hazards Group Infrared Precipitation (CHIRP) estimates. The merging algorithm uses residual inverse distance weighting for daily rainfall, and residual ordinary kriging for monthly rainfall. More details are given by Aybar et al. (2020). Another dataset for Peru and Ecuador with a spatial resolution of 0.1° (RAIN4PE; Fernandez-Palomino et al., 2022) was published after we started with the present work. We found that rainfall sums in the Chirilu catchments from this dataset are very similar, so we continued to use the PISCO dataset for comparison.

2.2.3 Other data

We use a global digital elevation model (DEM) with a spatial resolution of 30 m (ASTER Science Team, 2001). The DEM was used to determine a consistent set of station elevations. For the rainfall interpolation, the DEM was aggregated to 1000 m grid size.

Runoff data from the Chillón and Lurín catchments were obtained from the Peruvian Meteorological and Hydrological National Service (Servicio Nacional de Meteorología e Hidrología del Perú, SENAMHI).

3 Rainfall Patterns and Statistical Characteristics

Average annual rainfall is virtually zero at lower altitudes. Above a threshold elevation, annual rainfall increases almost linearly to around 700 mm per year on average at the highest stations (Figure 2). Fitting a piecewise linear regression with two segments (Muggeo, 2003) to the average annual rainfall of 16 stations with more than 360 months of data yields a linear increase above a breakpoint at 1515 m a.s.l. ($R^2 = 0.91$). Data from stations with shorter records confirm the increase of average rainfall with elevation, but show a larger spread (Figure 2 a). There is no indication of temporal trends in average annual rainfall sums over the observation period (water years 1964 to 2019; the water year in Peru is from September to August). The inter-annual variance of the rainfall is also increasing with elevation; a threshold elevation of around 1823 m was found with a segmented linear model of rainfall variance against elevation (16 stations, $R^2 = 0.60$; Figure 2 b).

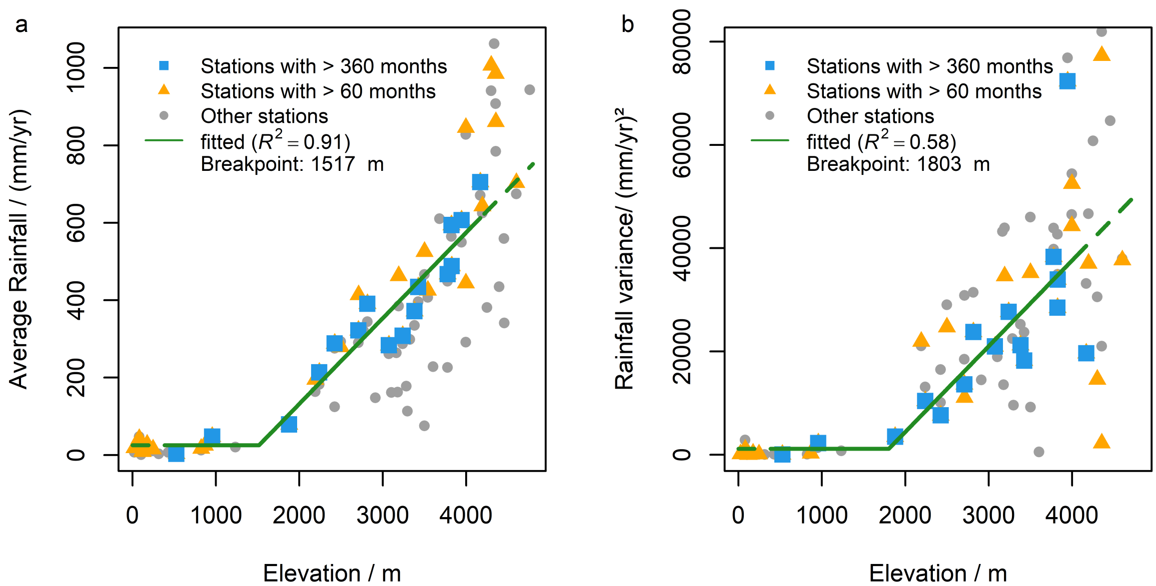

Figure 2: Annual rainfall in the study area in relationship to topography: average annual rainfall (a) and variance of rainfall (b) as a function of station elevation. Segmented linear functions (green lines) were fitted to the average and variance from 16 stations with more than 360 months of data (blue squares). Data from stations with more than 60 months of data are indicated by orange triangles; stations with shorter records are shown as grey points. Note b: 7 stations with shorter records exceed the upper axis limit for the rainfall variance.

The analysis of average rainfall per month, again based on stations with more than 30 data points for the respective month, confirms this dependency of rainfall on elevation above a certain threshold, and shows the seasonal pattern of rainfall (Figure 3). Seasonal averages of rainfall below the elevation threshold vary between 0.1 mm and 8.3 mm. During the rainy season from December until April, the elevation of this threshold varies between 766 m and 1818 m, and rainfall above the threshold increases to a maximum of over 150 mm per month on average. There is no significant rainfall during the dry season from May until September, except for minor rainfall above an elevation of around 3600 m. October and November can be regarded a transition period, with moderate rainfall occurring above 3100 m. We fitted piecewise linear functions to the long-term observations for each month (Figure 3).

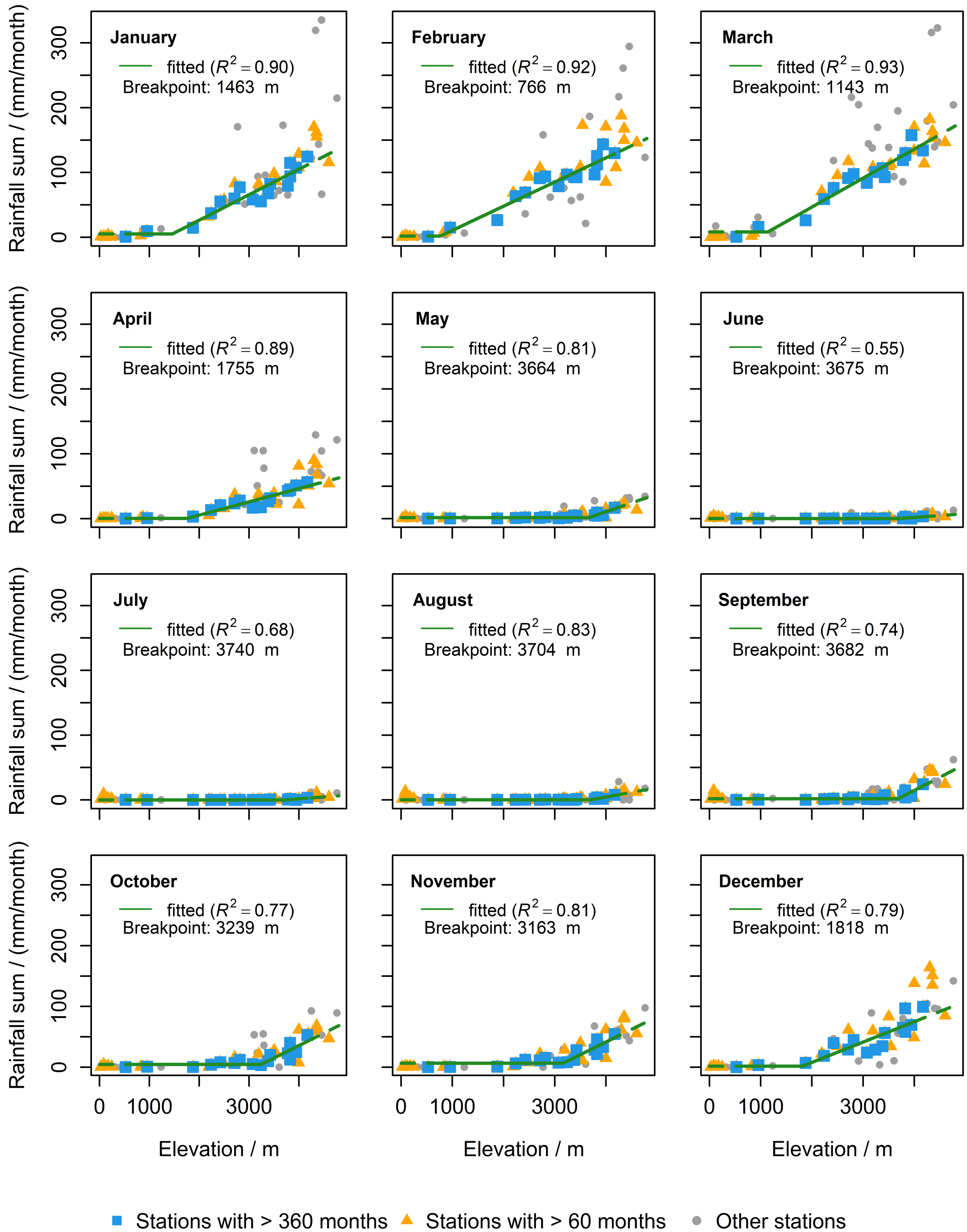

Figure 3: Average rainfall by months as a function of station elevation. Piecewise linear regressions (green lines) were fitted to the average rainfall from 16 stations with more than 30 complete records for this month (blue squares); the coefficient of determination and the breakpoint are given in each panel. Data from stations with more than 60 months of data are indicated by orange triangles; stations with shorter records by grey points.

To further assess spatial patterns, we looked at the spatial covariance of the rainfall after detrending the elevation dependency, and analyzed experimental variograms of different subsets of the data. Variograms describe the decline in statistical dependence with increasing separating distance of point pairs, which implies that the semivariance should grow monotonously with separating distance. This was not found, however, in the Chirilu rainfall dataset. The semivariance of the residuals - the deviation of the average annual rainfall at a station from the mean average rainfall expected at the elevation of the station – revealed pure nugget variograms (Figure 4 a, b), regardless of whether the 16 stations with long-term data, or all 67 stations were used. Fitting of theoretical variograms hence cannot provide a robust basis for spatial interpolation in this case. Similar results were obtained for variograms with average annual rainfall before detrending, and with mean monthly rainfall using the 16 long-term stations. Better variograms were obtained for the mean monthly rainfalls using all 67 stations, although the quality of the experimental variograms differed between the months. The semivariances again were consistently larger for all stations compared to the variogram analysis using only the long-term stations. We also analysed residuals for the monthly and daily data, respectively, which again yielded mixed results. Variograms without clear statistical dependence were found for 236 of 406 months with more than 20 stations (58 %), and for 104 of 198 days with more than 40 stations (53 %). Neither the use of the Cressie-Hawkins-estimator, nor of ranked variograms yielded any improvement.

We nevertheless found useful spatial relationships, when analyzing the correlation coefficient, which shows a systematic decline with the absolute value of the elevation difference (Figure 4 d). The relationship with separating distance is less strong (Figure 4 c). We explain this to be a consequence of the dependence of rainfall on elevation: two stations may experience a similar rainfall input not only if they are close to each other, but also if they are located at comparable elevations. The larger the difference in their elevation, the less correlated the rainfall records of two stations will be. This seems not necessarily the case when using the map distance of the stations.

The low quality of the variograms made kriging appear unsuitable for interpolating the rainfall data. In consequence, we developed a different means to interpolate the rainfall data that makes use of the relationships of average rainfall and rainfall variance with elevation and the correlation as a function of elevation difference, as detailed in the next section.

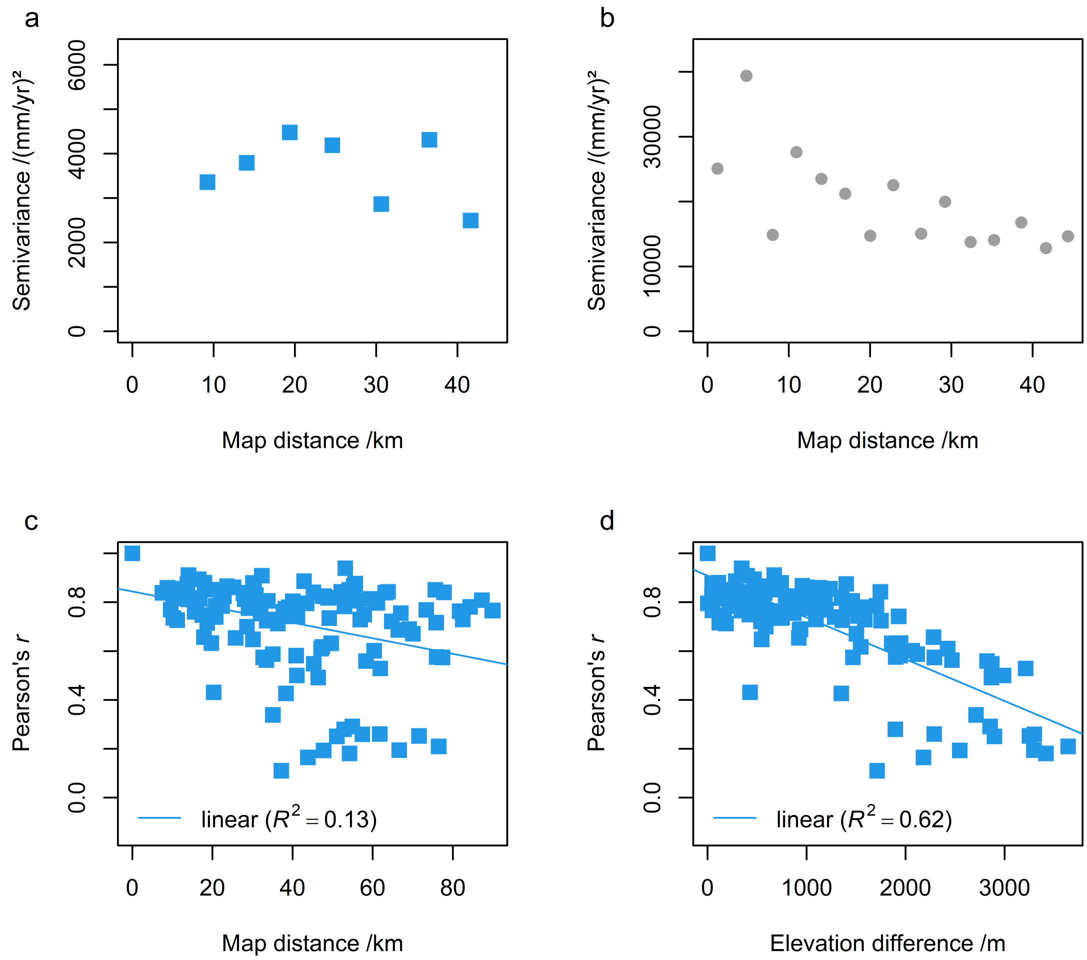

Figure 4: Spatial patterns in observed rainfall: Experimental variograms of average annual rainfall, detrended from the dependency with elevation: a) based on data from long-term series (16 stations with > 360 months of data), b) based on all available data (67 stations). Correlation (Pearson's correlation coefficient) of monthly rainfall sums of 16 long-term stations (> 360 months of data) against map distance (c), and against absolute difference in elevation (d).

4 β-IDW Model for Rainfall Interpolation

For mapping rainfall over the study area, we employ a Reynolds decomposition: the precipitation estimate $\hat{P}(x_i,t)$ at a certain point x_i and time t is expressed as the sum of the average rainfall that is expected according to elevation z at this point, $\bar{P}(z(x_i),t)$, and a temporal fluctuation from this average, $P'(x_i,t)$:

$$\hat{P}(x_i,t) = \bar{P}(z(x_i),t) + P'(x_i,t)$$

1)

The average expected rainfall per month is determined from the piecewise linear regression for the respective month (Figure 3). For daily estimates, the expected rainfall sum per day is determined by dividing by the average number of rain days of the month.

The deviation of the precipitation sum from its elevation-dependent average at a specific location and time step, $P'(x_i, t)$, is estimated from the deviation at an observation station, $P'(x_j, t)$

$$P'(x_i, t) = \beta(h) \cdot P'(x_j, t) \tag{2}$$

where β is a scaling parameter that depends on the elevation difference $h = z(x_i) - z(x_j)$ between the interpolation location and the observation station.

The scaled deviations from *n* stations are interpolated with IDW to get an estimate for the interpolation location:

$$\hat{P}'(x_i, t) = \frac{\sum_{j=1}^{n} d_{ij}^{-\lambda} \beta_j(h_{ij}) \cdot P'(x_j, t)}{\sum_{j=1}^{n} d_{ij}^{-\lambda}} \tag{3}$$

where d_{ij} are Euclidian distances, and λ is the power parameter.

The scaling with β reflects the increase in variance with the elevation. The estimate for the deviation from the mean should be higher than the observed deviation if the observation station is at a lower elevation than the interpolation point ($\beta > 1$), and lower if the observation is from a higher station. We found the following metric useful, which scales the covariance of two rainfall stations by the variance of one of the stations:

$$\beta(h_{kl}) = \frac{\mathrm{cov}(P(x_k), P(x_l))}{\mathrm{var}(P(x_k))} \tag{4}$$

where $P(x_k)$ and $P(x_l)$ are observed rainfall time series at two different locations, and cov and var denote covariance and variance, respectively. Unlike the correlation matrix, the matrix of scaling factors $\boldsymbol{\beta}$ is not symmetrical, which reflects the importance of the direction of the elevation difference given as $h_{kl} = z(x_k) - z(x_l)$.

This metric has gained considerable attention in economics as the "*beta*", which measures how an individual asset changes compared to changes in the overall stock market. This use dates back to the capital asset pricing model of Sharpe and Lintner in the 1960s (cf. Fama & French, 2004; Sharpe, 1991).

Using the statistical-topographical β-IDW model for daily rainfall interpolation over a grid includes the following steps for each raster cell *i*:

- determine the expected rainfall for that day according to the average monthly precipitation estimated for the elevation and month (Figure 3), divided by the average number of rain days for that month,
- find the nearest *n* stations with data on that day, and determine their expected rainfall according to elevation, the deviation of the observed rainfall on that day, as well as map distances d_{ij}, elevation differences h_{ij}, and scaling factors $\beta_j(h_{ij})$ (Figure 5),

- interpolate the scaled deviations from the stations to the interpolation point using eq. (3), and get the rainfall estimate for that day by summing the expected rainfall and the interpolated actual deviation.

5 Results and Discussion

5.1 Parameterization of the scaling factor β

For our case study, the relationship of β_{kl}, eq. (4), and the elevation difference, h_{kl}, was analyzed using monthly rainfall time series of stations with average annual rainfall larger than 5 mm (Figure 5). Functional relationships were established using 15 long-term stations; one station with less than 5 mm average annual rainfall was excluded. Stations with shorter records again showed larger scatter. Two functions were chosen for further analysis: a linear regression forced to pass through (0, 1) to ensure an unbiased estimate when the elevation difference is zero (L01; $R^2 = 0.75$), and a segmented linear regression with two breakpoints (SLR; $R^2 = 0.84$). Other regression functions (unconstrained linear, exponential, cubic polynomial, and local polynomial regression) yielded coefficients of determination in between these two models.

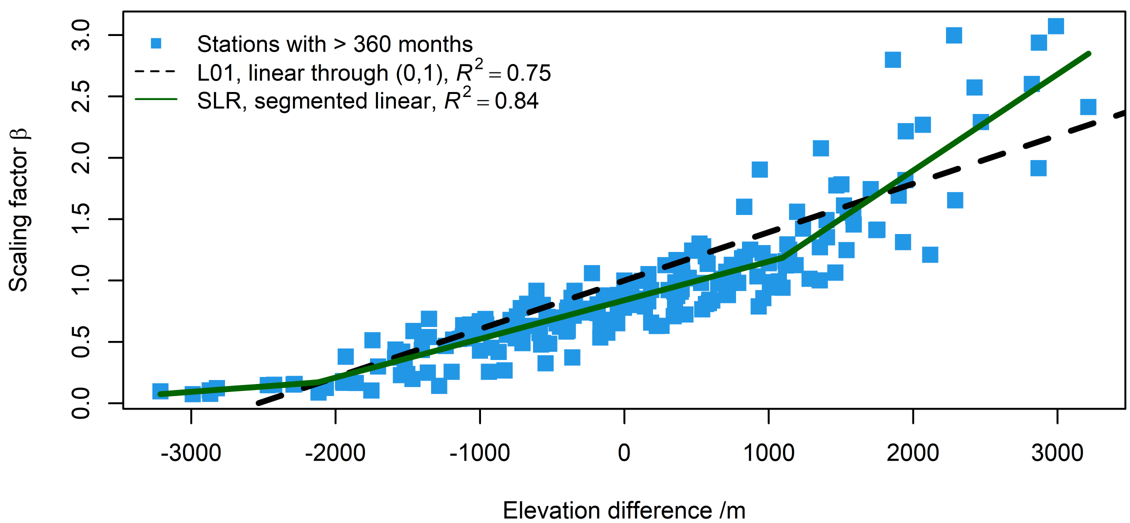

Figure 5: Scaling factor β from monthly rainfall series as a function of elevation difference; regression functions L01 and SLR (linear through (0, 1), and piecewise linear with three segments, respectively) were fitted using the long-term stations with 360 or more months of data. Only stations with average annual rainfall larger than 5 mm were considered.

5.2 Leave-one-out cross-validation

Suitable values for the number n of neighboring stations and the power parameter λ for the application of β-IDW to the study area were found through leave-one-out cross-validation. For this we used days with more than seven rainfall stations, which corresponds to 98 % of the study period (19933 days between 1 January 1964 and 28 September 2019). The minimum of n or the number of available stations of either day was used in the cross-validation.

The combination with the lowest mean absolute errors (MAE) across all stations was found for L01 with n = (4, 6) and λ = 1 (median MAE of 0.71 mm/d), and for SLR with n = 4 and λ = (0.5, 1) (median MAE of 0.76 mm/d). A conventional IDW interpolation with these parameters yielded a median MAE of 0.79 mm/d; the lowest median MAE of the classic IWD interpolations was 0.75 mm/d with n = 6 and λ = 1 (Table 1). We used the combinations with the lowest MAE for the β-IDW and the conventional IDW interpolation, respectively.

The cross-validation MAE are generally higher at higher elevations. For example, the median MAE for the IWG stations in the cross-validation with the selected parameter combinations were 2.26 mm/d, 2.27 mm/d and 2.51 mm/d for L01, SLR and conventional IDW, respectively. Overall, the cross-validation suggests a comparable performance of the methods at the location of the stations, indicating that no additional bias is introduced by the β-IDW approach. Still there are notable differences in the spatial patterns and estimated rainfall sums in unobserved parts of the catchments, as detailed in the next sections.

Table 1: Cross-Validation Results: Mean Absolute Error (MAE) As a Function of the Number of Points n and IDW Distance Exponent λ for β-IDW and Conventional IDW

n	β-IDW (L01) λ				β-IDW (SLR) λ				Conventional IDW λ			
	0.5	1	2	5	0.5	1	2	5	0.5	1	2	5
1	0.98	0.98	0.98	0.98	0.98	0.98	0.98	0.98	0.84	0.84	0.84	0.84
2	0.77	0.77	0.77	0.81	0.8	0.8	0.8	0.82	0.82	0.81	0.82	0.81
4	0.72	**0.71**	0.75	0.81	0.76	**0.76**	0.78	0.79	0.8	0.79	0.78	0.8
6	0.75	0.71	0.74	0.81	0.79	0.77	0.76	0.79	0.77	**0.75**	0.77	0.8
8	0.76	0.73	0.74	0.81	0.77	0.77	0.77	0.8	0.84	0.8	0.76	0.8
10	0.76	0.74	0.74	0.81	0.77	0.77	0.77	0.8	0.85	0.8	0.79	0.8

Note. Values are median MAE of daily rainfall across all stations. Combinations highlighted in bold were chosen for following interpolations.

5.3 Rainfall maps

We applied the β-IDW model to map rainfall for the Chirilu catchments in the continuous period from 1 September 1999 to 1 December 2019 on a 1000 m grid. Figure 6 shows rainfall maps for the day with the maximum rainfall recorded at one station (24 January 2006), and the day of the maximum rainfall sum over all stations (9 February 2016), respectively. These examples illustrate how the patterns obtained with β-IDW are influenced by the combination of topography and rainfall stations (Figure 6 a, b, e, f), compared to the conventional IDW interpolation (Figure 6 d, h) that is based on station data only.

Differences between L01 and SLR are hardly discernible in the maps. Depending on the configuration of stations on a particular day, L01 may yield slightly larger extents of the area of maximum rainfall compared to SLR, due to the threshold parameterization of SLR (Figure 6 a, b).

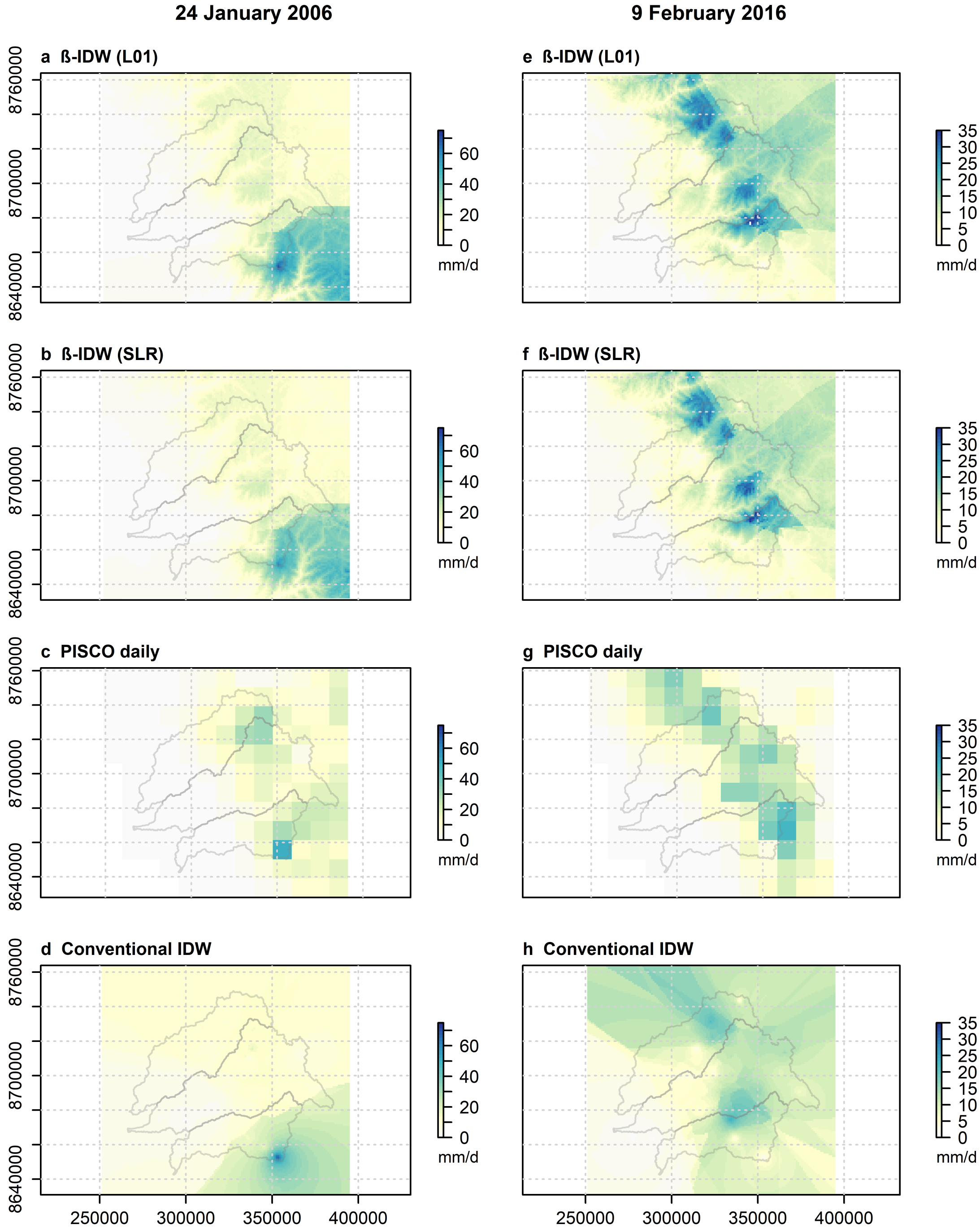
24 January 2006
9 February 2016
a ß-IDW (L01)
b ß-IDW (SLR)
c PISCO daily
d Conventional IDW
e ß-IDW (L01)
f ß-IDW (SLR)
g PISCO daily
h Conventional IDW
mm/d
8640000
8700000
8760000
250000
300000
350000
400000

396

Figure 6: Rainfall maps for the day with maximum rainfall observed at one station (24 January 2006; 74 mm/d at San Lazaro de Escomarca, a-d), and the day with the maximum rainfall sum over all stations (9 February 2016; median station rainfall 10.8 mm/d, maximum station rainfall 24.4 mm/d, e-h): Statistical-topographic model β-IDW with parameterization L01 (a, e) and SLR (b, f), PISCO precipitation product (c, g), and conventional IDW interpolation (d, h). Only stations inside the Chirilu catchments were used for mapping, except for PISCO. The catchment outlines are given as reference; coordinates are in m (WGS 1984, UTM Zone 18S).

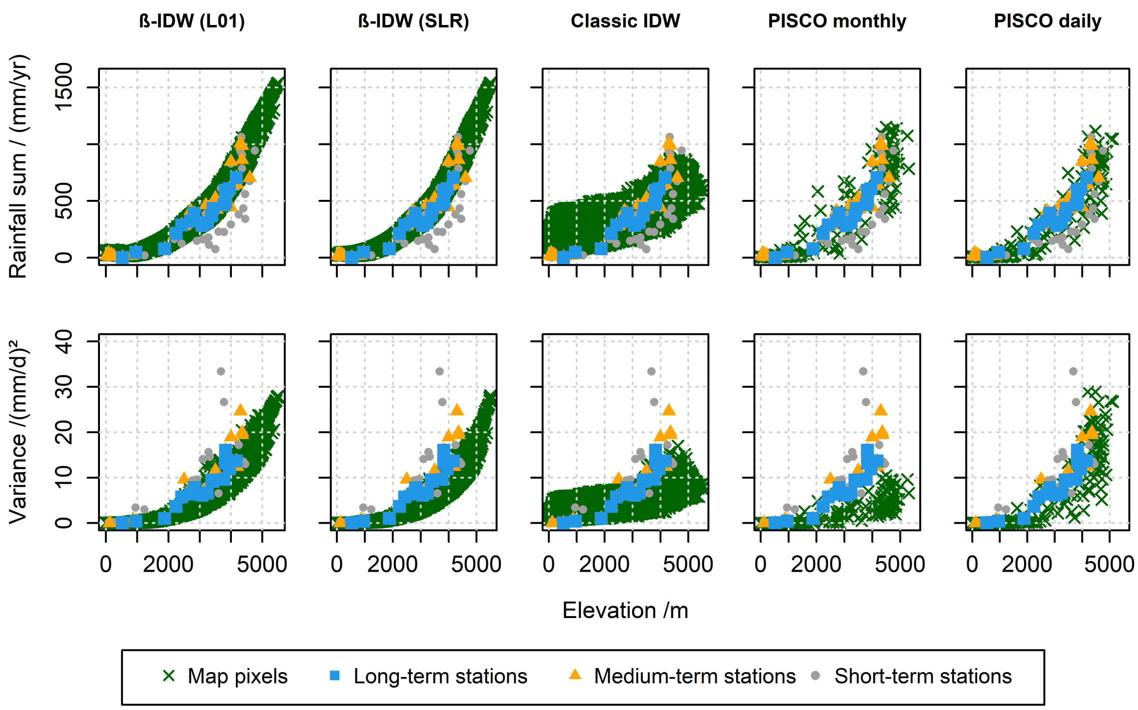

Figure 7: Comparison of observed and mapped rainfall in the period 1 September 1999 to 1 December 2019: average annual rainfall (top row) and variance (bottom row) as modelled with β-IDW (L01), β-IDW (SLR), classic IDW, and monthly and daily PISCO products, respectively. The observation stations are in the same categories as in Figure 2.

The rainfall patterns modeled with β-IDW are roughly similar to PISCO when looking at the Chirilu catchments, where the rainfall stations that were used for β-IDW are located. The results outside of the Chirilu area are to be taken with caution and will not be considered further. The rainfall fields in the catchments correspond quite well in terms of their extent, while the location and the magnitude of the highest rainfall rates differ. The coarser resolution of the PISCO products can be one factor for this; another factor is that β-IDW scales the local deviations with the elevation difference to the observation stations, which leads to higher rainfall intensities at unobserved locations (Figure 6).

This is also evident when looking at the distribution of average annual rainfall of the map pixels (Figure 7, top row). The β-IDW models extrapolate the trend of increasing rainfall with elevation, whereas the other methods hardly yield values outside the observed range, and thus possibly underestimate rainfall at higher elevations. The conventional IDW interpolation also fails to reproduce the trend in the other direction accurately and overestimates average rainfall at lower elevations.

The variance in the precipitation estimates from the β-IDW models matches well with the observed increase of variance with elevation, in particular at elevations below 4000 m. At higher elevations, the increase of the variance is not as steep as observed (Figure 7, bottom row). The daily PISCO product also matches the observed variance well. The increasing trend of the variance with elevation is not reproduced as well by the monthly PISCO product and the conventional IDW interpolation (Figure 7, bottom row).

5.4 Catchment-scale rainfall

5.4.1 Comparison of rainfall mapping methods

Two gauged subcatchments in the Lurín (gauge Puente Antapucro, 1047 m a.s.l.) and the Chillón (gauge Puente Magdalena, 875 m a.s.l.) were chosen to assess the suitability of the rainfall mapping for catchment-wide rainfall input for the water years 2000-2019. They are similar in size and orientation, and both are covering the middle and upper parts of their basins where precipitation actually occurs.

The annual areal precipitation inputs obtained with the β-IDW models are higher than those from the other methods in most years (Figure 8). Total areal rainfall is highest for L01, while SLR yields 97 % and 98 % of L01 in the Lurín and Chillón subcatchments, respectively. For the Lurín subcatchment, the mean annual rainfall input with conventional IDW, monthly and daily PISCO is only 62 % (63 %), 83 % (85 %), and 70 % (72 %) of the L01 (SLR) rainfall total, respectively. For the Chillón, conventional IDW, monthly and daily PISCO are on average 77 % (78 %), 92 % (94 %) and 84 % (86 %) of the L01 (SLR) rainfall total, respectively. The only exceptions are the water years 2018, in which monthly PISCO has higher areal rainfall input to both Lurín and Chillón compared to β-IDW, and 2019, in which conventional IDW exceeds the β-IDW estimates for the Chillón subcatchment.

These consistently higher estimates are a result of the extrapolating property of the β-IDW method to unobserved locations at higher altitudes. The differences to the other methods are thus smaller in the Chillón catchment, where more rain gauges are located at higher elevations compared to the Lurín (Figure 1), and the need for extrapolation is smaller.

Despite their difference in rainfall totals, the different methods produce a similar interannual variation of rainfall totals, as shown by their correlations to each other. The annual rainfall time series modeled with β-IDW-L01 and β-IDW-SLR are very highly correlated (r = 0.998); the same applies for daily and monthly PISCO products (r = 0.995). The correlation of conventional IDW is highest with daily PISCO (r = 0.952), but lowest with monthly PISCO (r = 0.796). Daily PISCO also involves IDW interpolation, while the monthly PISCO is based on

Kriging. The correlation of conventional IDW with the β-IDW models, however, is not as high (r = 0.820 to 0.848), and comparable to monthly PISCO (r = 0.796). The correlation coefficients reported are mean values for the two subcatchments. Correlation coefficients are generally slightly smaller in the Lurín catchment, which can be attributed to the higher coverage with rain gauges in the Chillón catchment.

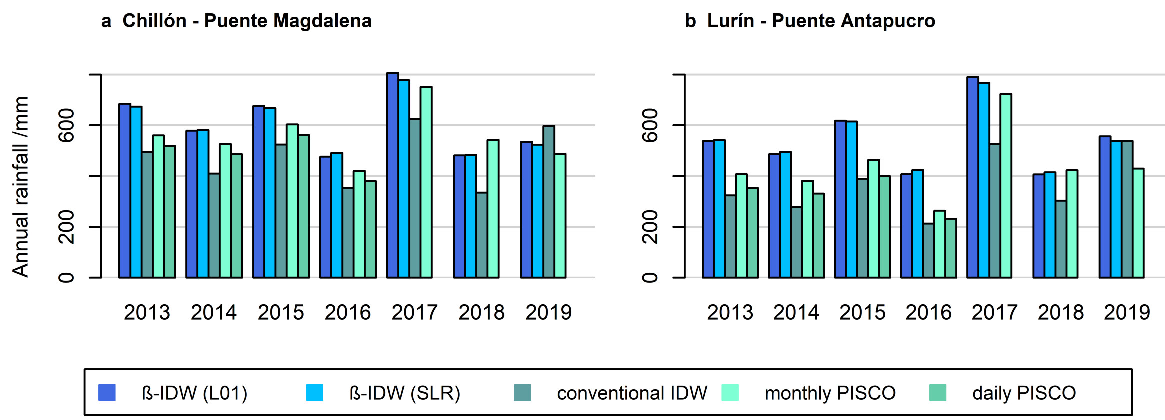

Figure 8: Annual areal rainfall inputs estimated with five different methods for the Puente Magdalena subcatchment of the Chillón (a) and the Puente Antapucro subcatchment of the Lurín (b). The dashed line denotes the average catchment input expected according to elevation (see Figure 3). PISCO with daily rainfall is only available until the end of 2016.

5.4.2 Evaluation using Rainfall-Runoff Ratios

Higher rainfall inputs, as with β-IDW appear plausible in light of hydrological data from the study area. During the studied time period, discharge observations are available for the water years 2002 to 2019 at Puente Magdalena (Chillón), except for 2012 and 2016, and for the water years 2015 to 2019 at Puente Antapucro (Lurín). These data were used to calculate annual rainfall-runoff ratios for the two sub-catchments (Table 2). The rainfall mappings with β-IDW yield the lowest rainfall-runoff ratio on average, with 0.25 and 0.39 for Chillón and Lurín, respectively. The other methods yield comparable, slightly higher ratios for Chillón (0.27 to 0.32), with β-IDW being closest to monthly PISCO. In the Lurín, β-IDW is also closest to monthly PISCO, which has an average rainfall-runoff ratio of 0.47, while the conventional IDW and daily PISCO are considerably higher (0.57 to 0.65; Table 2).

When interpreting the rainfall-runoff ratios and the differences between the neighboring catchments not only the rainfall mapping should be taken into account, but also the (unknown) uncertainty and the short length of the discharge data. It seems adequate to note, nevertheless, that higher rainfall input leading to lower rainfall-runoff ratios generally is more realistic for the studied catchments. A systematic underestimation of rainfall from daily PISCO and other QPE products was also found in a modeling study over 72 gauged catchments in the Peruvian and Ecuadorian Andes (Fernandez-Palomino et al., 2022), and correction factors increasing the rainfall by 43 % on average were needed to close the water balance, with the maximum bias located in the Ecuadorian Andes. Huerta (2020) reports average ratios of actual evapo-transpiration and precipitation in the period 2003 to 2013, which convert to average discharge ratios as low as 0.05 to 0.28 for the Pacific watersheds, and about 0.34 for entire Perú. The results of all QPE methods for the Chillón give runoff ratios within this range, while rainfall-runoff ratios for the Lurín all are higher, with the estimates using rainfall from β-IDW and monthly PISCO are much closer compared to the other methods in the Lurín (Table 2).

This is partly because the discharge station Puente Antapucro is located at a higher elevation, and most of the water abstraction and infiltration to the groundwater is downstream of the gauge. On the other hand, the density of rainfall gauges and the length of concurrent discharge series is greater in the Chillón catchment.

Table 2: Average Annual Rainfall-Runoff Ratios With the Different Rainfall Mapping Methods

	β-IDW L01	β-IDW SLR	Conventional IDW	PISCO monthly	PISCO daily
Chillón	0.25	0.25	0.32	0.27	0.30
Lurín	0.39	0.39	0.57	0.47	0.65

Note. Discharge data for 16 and 5 water years were available for the sub-catchments Puente Magdalena (Chillón) and Puente Antapucro (Lurín), respectively.

5.4.3 Effect of Including New Rain Gauges

Finally, we take the new IWG rain gauges, which are located at higher elevations in the Lurín subcatchment (Figure 1), as an example to analyze how station density affects the rainfall mapping. We compare the QPEs that are obtained with β-IDW and conventional IDW using the full data set to QPEs with a reduced data set, excluding the two and four rain gauges that measured in the headwaters of the Lurín catchment in the water years 2018 and 2019, respectively.

In 2018, both datasets give very similar results (Figure 9). All three methods estimate rainfall to be below the expected long-term elevation-dependent average, while the extrapolation to higher elevations leads to more rainfall from the β-IDW models compared to conventional IDW. The estimates are marginally higher with the reduced data set, which shows that the observations at the two new stations do not provide much new information except being slightly lower than at the other twelve stations.

In 2019, all three methods perform very similar with the full dataset, and catchment rainfall input is above the expected elevation-dependent average. This means that both the absolute rainfall and the deviations from the mean are higher for the four new stations than for the five other stations. Without the four additional stations, the estimated catchment rainfall is below the expected average, but still higher with β-IDW compared to conventional IDW (Figure 9).

The new stations are thus located at the "right" places, where rainfall info actually was lacking before. When the station density is lower and observations especially at higher altitudes are missing, the β-IDW approach provides a means to compensate partially for the underestimation of catchment precipitation that occurs when interpolating station data without any scaling. Including new stations at the right locations has a larger effect than the interpolation method in this case, which is consistent with other studies (Buytaert et al., 2006; Dirks et al., 1998; Michelon et al., 2021).

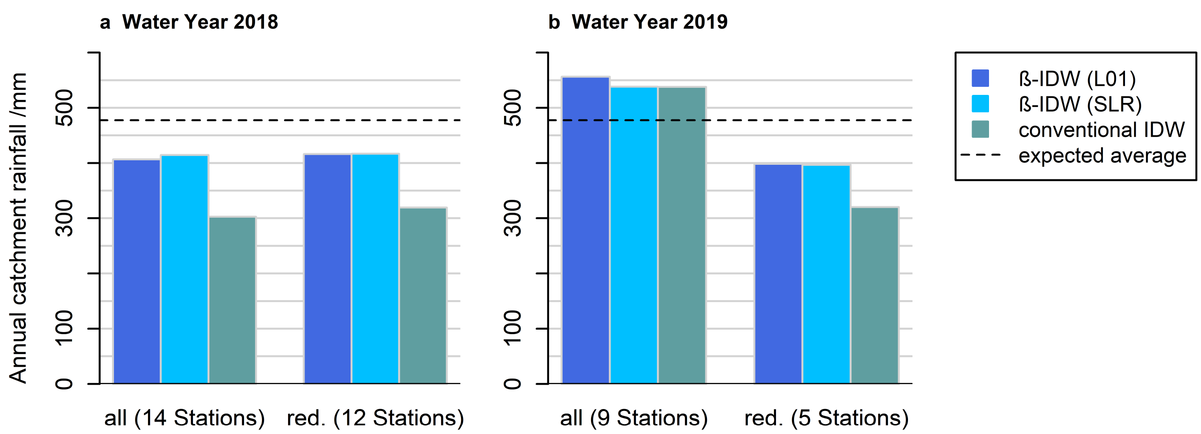

Figure 9: Catchment rainfall input for Lurín (Puente Antapucro) in the water years 2018 (a) and 2019 (b) with three mapping methods comparing the full dataset against a reduced dataset excluding the IWG stations in the headwater catchments. The dashed line denotes the expected annual catchment input according to pixel elevations for comparison.

6 Conclusions

We have presented an approach for mapping rainfall over mountainous catchments that is based on robust statistical relationships of rain gauge measurements with orographic elevation. The method uses daily rain gauge observations and models daily rainfall on a grid as the sum of the rainfall expected according to the elevation, and a deviation estimated from adjacent rain gauges. A key feature of the method is the scaling of the residuals according to their difference in elevation to the interpolation point. For the scaling we make use of the "beta" metric from economics, which is the covariance normalized with the variance. Because the deviation from the expected rainfall is finally calculated as the IDW interpolation of the scaled residuals, we named the method "β-IDW". Other forms of interpolation, especially Kriging, could also be applied to the scaled residuals, if meaningful variograms can be defined.

The development of β-IDW was motivated by our analysis of rainfall patterns in the Chirilu catchments near Lima, Peru. Geostatistical interpolation was hampered because consistent variograms could not be determined, neither with daily nor time-averaged data, even after detrending. We instead made use of other statistical relationships of long-term observations of rainfall and topography to include spatial correlations. Average monthly rainfall sums were well portrayed as a segmented linear function of elevation, and expected daily rainfall was obtained by dividing by the average number of rainy days for the respective month. For the scaling factor β we used linear and segmented linear functions of elevation difference. The interpolated rainfall was evaluated by cross-validation and comparison with the PISCO product of the Peruvian meteorological survey, and analysis at the sub-catchment level.

The results show that the β-IDW method can have advantages over other interpolation schemes when estimating rainfall input for mountainous catchments, where observations of higher rainfall at higher elevations are often underrepresented in the datasets. The β-scaling can overcome this limitation to a certain extent by its extrapolating property, as suggested by significantly higher rainfall input to the studied catchments with β-IDW than with conventional IDW, or more complex country-wide precipitation products, even though the latter incorporate both station observations and remote sensing information.

Our method is readily applicable to any mountainous region where station observations and a DEM in coarse resolution are available. Except for the preparatory statistical analyses and regressions, the (computational) time and effort for a β-IDW interpolation is comparable to a conventional IDW approach. The method is flexible, in the sense that any changes of the rain gauge network can be handled on a day-to-day basis, and new rain gauges can be included seamlessly. As shown for the Lurín catchment, using β-IDW with the long-term relationships mainly from the neighboring catchments can significantly improve the quantitative precipitation estimation for a sparsely gauged catchment. Even though we would suggest that installation of new rain gauges at appropriate locations still is the best way for reducing the uncertainty in rainfall estimates, the β-IDW approach can provide an alternative means for quantitative precipitation estimation in mountain catchments, also in other regions of the world.

The presented approach is useful for water resources management and related hydrological modelling at daily or longer time scales. If the β-scaling can also improve estimates of rainfall at higher temporal resolution for flood prediction and hydraulic modelling, possibly linked to approaches that explicitly consider the space-time behavior of rainfall fields, is subject for further research.

Acknowledgments

This work was partly funded by the German Federal Ministry of Education and Research under the grant number 02WGR1426A-G.

We thankfully acknowledge Samuel Schroers for the efforts of setting up (together with LA and JB) and maintaining the IWG rain gauges; Observatorio del Agua Chillón Rímac Lurín for sharing their data collection; Ana Brankovan for helping with data curation; and András Bárdossy for constructive comments during early stages of the study.

Open Research

The source code and curated data to reproduce the figures and analyses in this paper is available from HydroShare (Wienhöfer, 2023), licensed as CC-BY 4.0.

Rainfall data were taken from a data set provided by Observatorio del Agua Chillón Rímac Lurín; except for the data of the IWG rain gauges, which are from the LAMA data set (Schroers et al., 2021), available under a CC-BY 4.0 license.

Elevation data were taken from AST14DEM v003 (ASTER Science Team, 2001).

Discharge data were retrieved on 6 October 2021 from the SENAMHI web page: http://app.senamhi.gob.pe:9090/SISGESHIDRO/monitoreo_caudal.jsp.

For data analysis, coding of the rainfall interpolation and production of the graphics we used the R software, version 4.1.2 (R Core Team, 2021), including the packages "corrplot" (Wei & Simko, 2021), "doParallel" (Microsoft Corporation & Weston, 2020a), "foreach" (Microsoft Corporation & Weston, 2020b), "gstat" (Pebesma, 2004), "hydroTSM" (Zambrano-Bigiarini, 2020b), "hydroGOF" (Zambrano-Bigiarini, 2020a), "lubridate" (Grolemund & Wickham, 2011), "RANN" (Arya et al., 2019), "raster" (Hijmans, 2021), "rgdal" (Bivand et al., 2021), "rts" (Naimi, 2021), "segmented" (Muggeo, 2008) , and "zoo" (Zeileis & Grothendieck, 2005).

References

AghaKouchak, A., Behrangi, A., Sorooshian, S., Hsu, K., & Amitai, E. (2011). Evaluation of satellite-retrieved extreme precipitation rates across the central United States. *Journal of Geophysical Research: Atmospheres, 116*(D2). doi: https://doi.org/10.1029/2010JD014741

Anagnostou, E. N. (2004). Overview of overland satellite rainfall estimation for hydro-meteorological applications. *Surveys in Geophysics, 25*(5-6), 511-537. doi: 10.1007/s10712-004-5724-6

Arya, S., Mount, D., Kemp, S. E., & Jefferis, G. (2019). RANN: Fast Nearest Neighbour Search (Wraps ANN Library) Using L2 Metric. Retrieved from https://github.com/jefferis/RANN

ASTER Science Team. (2001). *ASTER DEM Product [Data set]*. NASA EOSDIS Land Processes DAAC. doi: 10.5067/ASTER/AST14DEM.003.

Aybar, C., Fernández, C., Huerta, A., Lavado, W., Vega, F., & Felipe-Obando, O. (2020). Construction of a high-resolution gridded rainfall dataset for Peru from 1981 to the present day. *Hydrological Sciences Journal, 65*(5), 770-785. doi: 10.1080/02626667.2019.1649411

Belo-Pereira, M., Dutra, E., & Viterbo, P. (2011). Evaluation of global precipitation data sets over the Iberian Peninsula. *Journal of Geophysical Research: Atmospheres, 116*(D20). doi: https://doi.org/10.1029/2010JD015481

Bivand, R., Keitt, T., & Rowlingson, B. (2021). rgdal: Bindings for the Geospatial Data Abstraction Library. Retrieved from https://CRAN.R-project.org/package=rgdal

Buytaert, W., Celleri, R., Willems, P., Bièvre, B. D., & Wyseure, G. (2006). Spatial and temporal rainfall variability in mountainous areas: A case study from the south Ecuadorian Andes. *Journal of Hydrology, 329*(3), 413-421. doi: https://doi.org/10.1016/j.jhydrol.2006.02.031

Campling, P., Gobin, A., & Feyen, J. (2001). Temporal and spatial rainfall analysis across a humid tropical catchment. *Hydrological Processes, 15*(3), 359-375. doi: https://doi.org/10.1002/hyp.98

Daly, C., Neilson, R. P., & Phillips, D. L. (1994). A statistical-topographic model for mapping climatological precipitation over mountainous terrain. *Journal of Applied Meteorology, 33*(2), 140-158. doi: 10.1175/1520-0450(1994)033<0140:ASTMFM>2.0.CO;2

Dirks, K. N., Hay, J. E., Stow, C. D., & Harris, D. (1998). High-resolution studies of rainfall on Norfolk Island Part II: Interpolation of rainfall data. *Journal of Hydrology, 208*(3-4), 187-193. doi: 10.1016/s0022-1694(98)00155-3

Ehret, U., Götzinger, J., Bárdossy, A., & Pegram, G. G. S. (2008). Radar-based flood forecasting in small catchments, exemplified by the Goldersbach catchment, Germany. *International Journal of River Basin Management, 6*(4), 323-329. doi: 10.1080/15715124.2008.9635359

Fama, E. F., & French, K. R. (2004). The Capital Asset Pricing Model: Theory and Evidence. *Journal of Economic Perspectives, 18*(3), 25-46. doi: 10.1257/0895330042162430

Fernandez-Palomino, C. A., Hattermann, F. F., Krysanova, V., Lobanova, A., Vega-Jácome, F., Lavado, W., et al. (2022). A Novel High-Resolution Gridded Precipitation Dataset for Peruvian and Ecuadorian Watersheds: Development and Hydrological Evaluation. *Journal of Hydrometeorology, 23*(3), 309-336. doi: 10.1175/jhm-d-20-0285.1

Garreaud, R. D. (2009). The Andes climate and weather. *Advances in Geosciences, 22*, 3. doi: https://doi.org/10.5194/adgeo-22-3-2009

Germann, U., Galli, G., Boscacci, M., & Bolliger, M. (2006). Radar precipitation measurement in a mountainous region. *Quarterly Journal of the Royal Meteorological Society, 132*(618), 1669-1692. doi: https://doi.org/10.1256/qj.05.190

Goovaerts, P. (2000). Geostatistical approaches for incorporating elevation into the spatial interpolation of rainfall. *Journal of Hydrology, 228*(1), 113-129. doi: https://doi.org/10.1016/S0022-1694(00)00144-X

Grolemund, G., & Wickham, H. (2011). Dates and Times Made Easy with lubridate. *Journal of Statistical Software, 40*(3), 1-25. doi: https://doi.org/10.18637/jss.v040.i03

Heistermann, M., & Kneis, D. (2011). Benchmarking quantitative precipitation estimation by conceptual rainfall-runoff modeling. *Water Resources Research, 47*(6). doi: 10.1029/2010WR009153

Herrera, S., Kotlarski, S., Soares, P. M. M., Cardoso, R. M., Jaczewski, A., Gutierrez, J. M., & Maraun, D. (2019). Uncertainty in gridded precipitation products: Influence of station density, interpolation method and grid resolution. *International Journal of Climatology, 39*(9), 3717-3729. doi: 10.1002/joc.5878

Hijmans, R. J. (2021). raster: Geographic Data Analysis and Modeling. Retrieved from https://rspatial.org/raster

Hofstra, N., Haylock, M., New, M., Jones, P. D., & Frei, C. (2008). Comparison of six methods for the interpolation of daily, European climate data. *Journal of Geophysical Research, 113*. doi: https://doi.org/10.1029/2008JD010100

Hu, Q. F., Li, Z., Wang, L. Z., Huang, Y., Wang, Y. T., & Li, L. J. (2019). Rainfall Spatial Estimations: A Review from Spatial Interpolation to Multi-Source Data Merging. *Water, 11*(3). doi: 10.3390/w11030579

Huerta, A. (2020). Vulnerabilidad de la disponibilidad de los recursos hidricos en el Peru frente al cambio climiatico: Analisis probabilistico de Budyko. In W. S. Lavado Casimiro (Ed.), *Estudios Hidrólogicos del SENAMHI: Resúmenes Ejecutivos - 2020* (pp. 88-96). Lima, Peru: Servicio Nacional de Meteorología e Hidrología del Perú, SENAMHI. doi: https://hdl.handle.net/20.500.12542/472.

Lavado Casimiro, W. S., Ronchail, J., Labat, D., Espinoza, J. C., & Guyot, J. L. (2012). Basin-scale analysis of rainfall and runoff in Peru (1969–2004): Pacific, Titicaca and Amazonas drainages. *Hydrological Sciences Journal, 57*(4), 625-642. doi: 10.1080/02626667.2012.672985

Li, J., & Heap, A. D. (2014). Spatial interpolation methods applied in the environmental sciences: A review. *Environmental Modelling & Software, 53*, 173-189. doi: https://doi.org/10.1016/j.envsoft.2013.12.008

Ly, S., Charles, C., & Degré, A. (2011). Geostatistical interpolation of daily rainfall at catchment scale: the use of several variogram models in the Ourthe and Ambleve catchments, Belgium. *Hydrol. Earth Syst. Sci., 15*(7), 2259-2274. doi: 10.5194/hess-15-2259-2011

Ly, S., Charles, C., & Degré, A. (2013). Different methods for spatial interpolation of rainfall data for operational hydrology and hydrological modeling at watershed scale: a review. *Biotechnologie, Agronomie, Société et Environnement, 17*(2), 392–406

Michaelides, S., Levizzani, V., Anagnostou, E., Bauer, P., Kasparis, T., & Lane, J. E. (2009). Precipitation: Measurement, remote sensing, climatology and modeling. *Atmospheric Research, 94*(4), 512–533. doi: https://doi.org/10.1016/j.atmosres.2009.08.017

Michelon, A., Benoit, L., Beria, H., Ceperley, N., & Schaefli, B. (2021). Benefits from high-density rain gauge observations for hydrological response analysis in a small alpine catchment. *Hydrol. Earth Syst. Sci., 25*(4), 2301-2325. doi: 10.5194/hess-25-2301-2021

Microsoft Corporation, & Weston, S. (2020a). doParallel: Foreach Parallel Adaptor for the parallel Package. Retrieved from https://CRAN.R-project.org/package=doParallel

Microsoft Corporation, & Weston, S. (2020b). foreach: Provides Foreach Looping Construct. Retrieved from https://CRAN.R-project.org/package=foreach

Muggeo, V. M. (2003). Estimating regression models with unknown break-points. *Statistics in medicine, 22*(19), 3055–3071. doi: https://doi.org/10.1002/sim.1545

Muggeo, V. M. (2008). Segmented: an R package to fit regression models with broken-line relationships. *R news, 8*(1), 20–25

Naimi, B. (2021). rts: Raster Time Series Analysis. Retrieved from http://r-gis.net

Neuper, M., & Ehret, U. (2019). Quantitative precipitation estimation with weather radar using a data- and information-based approach. *Hydrology and Earth System Sciences, 23*(9), 3711-3733. doi: 10.5194/hess-23-3711-2019

Observatorio del Agua Chillón Rímac Lurín. (2019). *Diagnóstico Inicial para el Plan de Gestión de Recursos Hídricos de las cuencas Chillón, Rímac, Lurín y Chilca*. Lima, Peru. Retrieved from http://observatoriochirilu.ana.gob.pe/publicaciones/diagnostico-inicial-para-el-plan-de-gestion-de-recursos-hidricos-en-las-cuencas

Pebesma, E. J. (2004). Multivariable geostatistics in S: the gstat package. *Computers & Geosciences, 30*, 683-691. doi: https://doi.org/10.1016/j.cageo.2004.03.012

R Core Team. (2021). R: A Language and Environment for Statistical Computing. Vienna, Austria: R Foundation for Statistical Computing. Retrieved from http://www.R-project.org

Roe, G. H. (2005). Orographic Precipitation. *Annual Review of Earth and Planetary Sciences, 33*(1), 645-671. doi: 10.1146/annurev.earth.33.092203.122541

Ruelland, D., Ardoin-Bardin, S., Billen, G., & Servat, E. (2008). Sensitivity of a lumped and semi-distributed hydrological model to several methods of rainfall interpolation on a large basin in West Africa. *Journal of Hydrology, 361*(1), 96-117. doi: https://doi.org/10.1016/j.jhydrol.2008.07.049

Scheel, M. L. M., Rohrer, M., Huggel, C., Santos Villar, D., Silvestre, E., & Huffman, G. J. (2011). Evaluation of TRMM Multi-satellite Precipitation Analysis (TMPA) performance in the Central Andes region and its dependency on spatial and temporal resolution. *Hydrol. Earth Syst. Sci., 15*(8), 2649-2663. doi: 10.5194/hess-15-2649-2011

Schroers, S., Bondy, J., & Wienhöfer, J. (2021). *Lurin Basin, Andean Measurement Campaign and Dataset (LAMA)* [Dataset]. doi: 10.5445/ir/1000130149.

Sharpe, W. F. (1991). Nobel Lecture : Capital Asset Prices with and without Negative Holdings. *The Journal of Finance, 46*(2), 489-509. doi: https://doi.org/10.1111/j.1540-6261.1991.tb02671.x

Sluiter, R. (2009). *Interpolation methods for climate data: literature review*. De Bilt, The Netherlands. Retrieved from https://cdn.knmi.nl/knmi/pdf/bibliotheek/knmipubIR/IR2009-04.pdf

Sun, Q. H., Miao, C. Y., Duan, Q. Y., Ashouri, H., Sorooshian, S., & Hsu, K. L. (2018). A Review of Global Precipitation Data Sets: Data Sources, Estimation, and Intercomparisons. *Reviews of Geophysics, 56*(1), 79-107. doi: 10.1002/2017rg000574

Trachte, K., Seidel, J., Figueroa, R., Otto, M., & Bendix, J. (2018). Cross-Scale Precipitation Variability in a Semiarid Catchment Area on the Western Slopes of the Central Andes. *Journal of Applied Meteorology and Climatology, 57*(3), 675–694. doi: https://doi.org/10.1175/JAMC-D-17-0207.1

Webster, R., & Oliver, M. A. (2007). *Geostatistics for environmental scientists*: John Wiley & Sons.

Wei, T., & Simko, V. (2021). corrplot: Visualization of a Correlation Matrix. Retrieved from https://github.com/taiyun/corrplot

Wienhöfer, J. (2023). *Material for 'Statistical-Topographical Mapping of Rainfall Over Mountainous Terrain Using Beta Scaling'* [Collection]. HydroShare. doi: 10.4211/hs.fa0007d553ae4c8682dd9c464e91913d.

Wienhöfer, J., Lindenmaier, F., & Zehe, E. (2011). Challenges in Understanding the Hydrologic Controls on the Mobility of Slow-Moving Landslides. *Vadose Zone Journal, 10*(2), 496-511. doi: 10.2136/vzj2009.0182

Young, C. B., Nelson, B. R., Bradley, A. A., Smith, J. A., Peters-Lidard, C. D., Kruger, A., & Baeck, M. L. (1999). An evaluation of NEXRAD precipitation estimates in complex terrain. *Journal of Geophysical Research: Atmospheres, 104*(D16), 19691-19703. doi: https://doi.org/10.1029/1999JD900123

Zambrano-Bigiarini, M. (2020a). hydroGOF: Goodness-of-Fit Functions for Comparison of Simulated and Observed Hydrological Time Series. doi: 10.5281/zenodo.839854. Retrieved from https://github.com/hzambran/hydroGOF

Zambrano-Bigiarini, M. (2020b). hydroTSM: Time Series Management, Analysis and Interpolation for Hydrological Modelling. Retrieved from https://github.com/hzambran/hydroTSM

Zeileis, A., & Grothendieck, G. (2005). zoo: S3 Infrastructure for Regular and Irregular Time Series. *Journal of Statistical Software, 14*(6), 1-27. doi: 10.18637/jss.v014.i06